J Mater Sci (2018) 53:1634–1645

Biomaterials

Mesoporous titanium dioxide@ zinc oxide–graphene oxide nanocarriers for colon-specific drug delivery

Mostafa Zamani[1], Mojtaba Rostami[2,3], Mozhgan Aghajanzadeh[1], Hamidreza Kheiri Manjili[4,5], Kobra Rostamizadeh[1,7], and Hossein Danafar[6,7,8,*]

[1] Department of Pharmaceutical Biomaterials, School of Pharmacy, Zanjan University of Medical Sciences, Zanjan, Iran
[2] Inter Islamic Network on Science and Technology Parks in Guilan, Rasht, Iran
[3] Nanotechnology Research Centre, Nano Alvand, Simindasht Industrial Area, Karaj, Iran
[4] Department of Pharmaceutical Nanotechnology, School of Pharmacy, Zanjan University of Medical Sciences, Zanjan, Iran
[5] Zanjan Pharmaceutical Biotechnology Research Center, Zanjan University of Medical Sciences, Zanjan, Iran
[6] Zanjan Pharmaceutical Nanotechnology Research Center, Zanjan University of Medical Sciences, Zanjan, Iran
[7] Cancer Gene Therapy Research Center, Zanjan University of Medical Sciences, Zanjan, Iran
[8] Department of Medicinal Chemistry, School of Pharmacy, Zanjan University of Medical Sciences, Zanjan, Iran

Received: 5 July 2017
Accepted: 5 October 2017
Published online: 13 October 2017

ABSTRACT

In this project, TiO_2@ZnO nanoparticles core–shell nanostructured and titanium dioxide@ mesoporous zinc oxide–graphene oxide (TiO_2@ZnO–GO) hybrid nanocomposites as controlled targeted drug delivery systems were synthesized by a facile sono-chemical method. We prepared a novel mesoporous and core–shell structure as a drug nanocarrier (NCs) for the loading and pH-responsive characteristics of the chemotherapeutic curcumin. The structure, surface charge, and surface morphology of NCs were studied using with X-ray diffraction, Fourier transform infrared spectroscopy, dynamic light scattering, brunauer–emmett–teller, scanning electron microscopy (SEM), and transmission electron microscopy (TEM). The SEM and TEM images of NCs show the uniform hexagonal mesoporous morphology with average grain size of about ~ 190 nm. The drug loading was very high about 16 and 19 for TiO_2@ZnO and TiO_2@ZnO–GO, respectively. The NCs showed pH-dependent drug release behavior. Drug release from TiO_2@ZnO–GO in neutral pH were higher than in acidic medium, due to anionic charge of GO nanosheet. MTT assay results showed that the curcumin-loaded NCs showed significant toxicity due to which cell viability reduced to below 50% at 140 μg/mL concentration, thereby confirming its anticancer effects. The goal of this study is the application of water-dispersed TiO_2@ZnO–GO with pH-dependent release properties for design a new drug delivery carrier.

Address correspondence to E-mail: Danafar@zums.ac.ir

DOI 10.1007/s10853-017-1673-6

Introduction

In 2016, over one and half million new cancer cases are diagnosed, and about six hundred thousand Americans were died of cancer the same year. Of these new cases in 2016, it is anticipated that one hundred thousands were be due to colon cancer. Indeed, colorectal cancer is the third leading reason of cancer death for both men and women [1]. However surgical removal of a primary colorectal tumor has proven to be beneficial, thirty percent of patients eventually develop a metastasis [2]. The most prevalent sites of metastasis are the liver, lungs, and draining lymph nodes [3]. Chemotherapy is one of the cancer therapy manners and many drugs such as irinotecan (CPT-11), doxorubicin (DOX), oxaliplatin (OXA), cisplatin (CP), and curcumin (CUR) have been used for chemotherapy [4–6].

CUR is the yellowish pigmentation of turmeric which is commonly used as a food flavoring and coloring agent. Its chemical formula is 1, 7-bis (4-hydroxy-3-methoxyphenyl)-1, 6-heptadiene-3,5-dione with a chemical structure in the keto-enol tautomerism [7, 8]. CUR is an attracting therapeutic agent from a pharmaceutical viewpoint because of its notable biological characteristics, including its antioxidant, antimicrobial, anti-inflammatory, and wound healing activities [9, 10]. It also displays potential use for the medicinal treatment of various diseases, especially cancer [11]. However, CUR suffers from some disadvantages including low water solubility under acidic or neutral conditions, high decomposition rate in an alkaline media, and photodegradation in organic solvents which subsequently limit its clinical applications [12]. The most challenging work in the progress of colon-specific drug delivery carriers is to deal with premature drug release from the carriers before the drug can be delivered to the target. To extend the successful colon-specific drug delivery NCs, they required to be stable and protected from the harsh acidic environment of the stomach and release the drug more specifically to the colon [13, 14]. Multiple approaches have been undertaken in recent years to develop the delivery of CUR in colonic tissues. Mucoadhesive chitosan nanoparticles [15], pH-sensitive nanoparticles [16], guar gum microspheres [17], polymeric NCs, [18] and graphene [19] have improved the bioavailability of CUR to some extent in colon, even so; these carriers did not deliver the soluble form of CUR.

Graphene (G), a two-dimensional single layer of carbon atoms in a closely packed honeycomb lattice, has attracted significant attention from scientific communities in recent years [20–22]. Graphene has been extensively studied in the last several years due to its interesting characteristics, such as significant electrical conductivity, great theoretical specific surface area and high chemical stability, excellent absorptivity, and excellent mechanical properties [23–25]. Graphene oxide (GO) is a derivative of graphene and has attracted attention of many bioapplications including cellular growth and differentiation [26], gene and drug delivery [27], and photo-thermal therapy [28]. GO can simultaneously activate toll-like receptor (TLR)-4 and -9 responses as same autophagy in macrophages [26] and colon cancer cell CT26. In addition, injection of GO alone stimulates the immune cell infiltration into the tumor bed and inhibits colon cancer growth in mice [29]. Furthermore, GO conjugated with chemotherapy drugs (DOX and CP-11) can improve the killing of MCF-7 cells that are resistant to DOX and CP [27].

Many research works are going on for the development of anticancer agents having enhanced targeted characteristics, better therapeutics and low toxicity [30–33]. Due to this, TiO_2@ZnO are regarded to be a promising substance because of its reported anticancer potential [34, 35]. TiO_2 is one of the well-known mesoporous materials. Because of biocompatibility, large surface area, and mesoporous properties of TiO_2, some of the investigation has been developed to use nanosized TiO_2 in dye-sensitized solar cells, electrochromic display, water splitting, degradation of organics, glucose sensors and specially as carrier for drug delivery which required slow and sustained release [36–38]. Biocompatibility and nontoxicity of TiO_2 caused by combination of TiO_2 with other materials such as mesoporous zinc oxide (mZnO) produce an intelligent drug delivery system for use in pharmaceutical formulation. In this work, we report the synthesis of a mesoporous TiO_2@ZnO and TiO_2@ZnO–GO by a facile sonochemical way to allow multifunctional properties to be imparted into such a nanostructure. CUR was loaded on NCs, and the loading capacity and release behavior of CUR from NCs were also tested. As expected, the prepared (TiO_2@ZnO–GO) have

displayed high anticancer drug loading and pH-sensitive release behavior.

Materials and methods

Material

Zinc (II) nitrate hexahydrate ($Zn(NO_3)_2$·$6H_2O$, ≥ 99%, $M_w = 290.70$ g/moL), CUR (Merck, Darmstadt, Germany, Art No. 820354), sodium hydroxide (NaOH, $M_w = 40$ g/moL), ethanol, and polyvinylpyrrolidone (PVP) surfactants were purchased from Merck. Deionized water was prepared by an ultra-pure water system (Smart-2-Pure, TKACo, Germany).GO was prepared from graphite powder using sulfuric acid (H_2SO_4, 98%), nitric acid (HNO_3, 98%), potassium permanganate ($KMnO_4$), 5% HCl, and hydrogen peroxide (H_2O_2, 30%), all purchased from Merck. Other solvents and chemicals were from chemical laboratory in purity grades.

Preparation of GO nanosheets

GO was synthesized from natural graphite powder by a modified Hummers method [35]. In a routine process, 1 g of graphite was added to 100 mL of concentrated H_2SO_4, 50 mL of HNO_3 in an ice bath, and while stirring, 4 g of $KMnO_4$ was slowly added. The reaction mixture is stirred for 2 h at temperatures below 10 °C, followed by 1 h at 35 °C until a thick dough had formed. After that, it is diluted by 100 mL of deionized (DI) water in an ice bath and transferred to a 98 °C oil bath and stirred for 1 h. Again, the mixture was diluted to 300 mL. Then, 20 mL H_2O_2 (30%) was added until the color of the solution changed to a light yellow. The final product was centrifuged and washed several times with 5% HCl solution, and then by DI water, until the supernatant became neutral. Finally, the final solid was dried at 60 °C for 24 h, and a loose brown powder was obtained.

Synthesis of TiO_2@ZnO–1 wt% GO and TiO_2@ZnO

At first, the TiO_2 nanoparticles were synthesized by the sol–gel method [39]. A mesoporous ZnO shell was coated on the TiO_2 nanoparticles using sonochemical method. In a typical procedure, 0.11 g of the TiO_2 nanoparticles was dispersed in a mixed solvent of ethanol: DI (1:1), 0.21 g PVP, and NaOH solution, followed by that, 1.8 g Zn $(NO_3)_2$·$6H_2O$ was added and exposed with ultrasound waves at room temperature for 5 h. Power and frequency of the ultrasound waves were 100 W and 20 kHz, respectively. Then, a suspension of 1 wt% of GO (prepared in mixture of 10 mL of DI and 20 mL of ethanol) was added to this solution at room temperature and stirred with magnetic stirring. The obtained ternary nanoparticles of TiO_2@ZnO–GO were dried at 100 °C overnight. For comparison, the same method was used to synthesize TiO_2@ZnO (m was short for mesoporous) with core–shell structure without GO.

Preparation of curcumin-loaded nanocarriers

CUR-loaded NCs were obtained by precipitation method by acetone as the solvent. Briefly, 15 mg of CUR was dissolved in 5 mL of acetone. Then, this solution was injected drop-wise into 50 mL of DI solution containing 60 mg of NCs under constant mixing rates and stirred magnetically at room temperature until complete evaporation of the acetone occurred and drug loaded nanoparticles were prepared. The final nanoparticles were separated by centrifuging at 20000 rpm for 15 min. The obtained NC was dried at vacuum oven overnight.

Characterization

XRD analysis

Phase analyses of the NCs were carried out by powder XRD (Philips X′ pert Pro MPD, Holland) using a graphite-filtered Cu Kα ($k = 0.9$ nm) radiation in the 2θ range of 10–90, at 2θ steps of 0.05, and a wavelength of 1.54 Å.

Particle morphology

The surface morphological properties of NCs were examined by means of scanning electron microscopy (SEM) (VEGA\\TESCAN-XMU) at an accelerating voltage of 20 kV, and transmission electron microscopy (TEM) images were obtained using a Philips CM120 microscope operating at 120 kV and linear resolution of 2.5 Å.

FT-IR analysis

FT-IR spectrophotometer (Bruker, Tensor 27, Biotage, Germany) was used for determining chemical structure of the NCs.

Determination of surface charge

The zeta potential of the prepared NCs was determined by dynamic light scattering (DLS) using a zetasizer (Malvern Instruments, Worcestershire, UK, model Nano ZS).

BET analysis

Nitrogen adsorption/desorption isotherms of TiO_2@ZnO were measured by a BELSORP-mini II adsorption porosimeter at 77 K after being degassed at 180 °C under vacuum for 5 h. The specific surface areas were calculated using the Brunauer–Emmett–Teller (BET) method, and the pore size distributions were calculated according to the Barrett–Joyner–Halenda (BJH) method.

Determination of loading efficiency

To determine the loading efficiency of the drug in the NCs, two parameters were determined including the drug loading ratio of drug. Drug loading ratio was determined as:

$$\mathrm{DL}\% = \frac{W_{\mathrm{drug}}}{W_{\mathrm{carrier}}} \times 100, \quad (1)$$

where DL% is the drug loading ratio (percent), and W_{drug} and W_{carrier} represent the weight of the entrapped drug and the total weight of the corresponding drug-entrapped carrier, respectively.

For determination of the drug loading ratio, 1 mg of the final dried NCs was dissolved in 1 mL of acetone, and the drug content was measured spectrophotometrically (Thermo Fisher Scientific, USA, Madison, model GENESYS™ 10S) at wavelengths of 420 nm.

Drug release study

In general, drug-loaded NCs are suspended in a vessel containing certain amount of release media, and then the drug release is investigated over time. Briefly, 5 mg of drug-loaded carriers were dispersed in 20 mL phosphate-buffered saline (PBS) containing 1% (v/v) Tween 80, and the resulting suspension incubated at 37 °C. The tubes were centrifuged at 12000 rpm for 5 min to separate the particles from medium, Then, at predetermined time intervals, 1 mL of the suspension was taken out and replaced by 1 mL fresh PBS. The concentration of CUR in the suspension was determined by ultraviolet–visible spectroscopy (UV–Vis) at wavelength of 420 nm. All the release studies were carried out in triplicate. In order to study the pH-dependency of the drug release, the experiments were carried out as well as at a pH of 5.5.

Cell cytotoxicity

For the MTT (3-[4,5-dimethylthiazol-2-yl]-2,5-diphenyl tetrazolium bromide) assay, 96 well plates were used, and Caco-2 cells were seeded onto plates and adhered and grown overnight in 200 µL culture medium with 10^4 cancer cells per well concentration. Then, the cancer cells were incubated with 100 µL fresh medium containing serial concentrations (0–140 µg/mL) of void CUR and same doses of CUR/TiO_2@ZnO–GO and CUR/TiO_2@ZnO for 24 h and a group without treatment for control. Then 20 µL of 4 mg/mL MTT solution was added to each 100 µL media of well and the plates were then incubated at 37 °C in a humidified atmosphere containing 95% air and 5% CO_2 for 3 h. Following the incubation, the MTT solution was eliminated, and 100 µL of dimethyl sulfoxide (DMSO) was added to each well for dissolution of the formazan crystals. The plates were shaken for 10 min on a plate shaker to obtain adequate solubility. After the shaking, absorbance readings of each well were done at 570 nm (single wavelength) by a multi-scan plate reader made in the UK. All experiments were repeated three times for statistical analysis. The final results were expressed as mean ± S.D.

Results and discussion

XRD

The Bragg diffraction peaks of the two NCs, shown in Fig. 1, agreed well with those of the pure synthesized hexagonal ZnO [40], at 2θ values of 31.9°, 34.6°, 36.4°, 47.7°, 56.8°, 63.0°, and 68.1° which were indexed to be

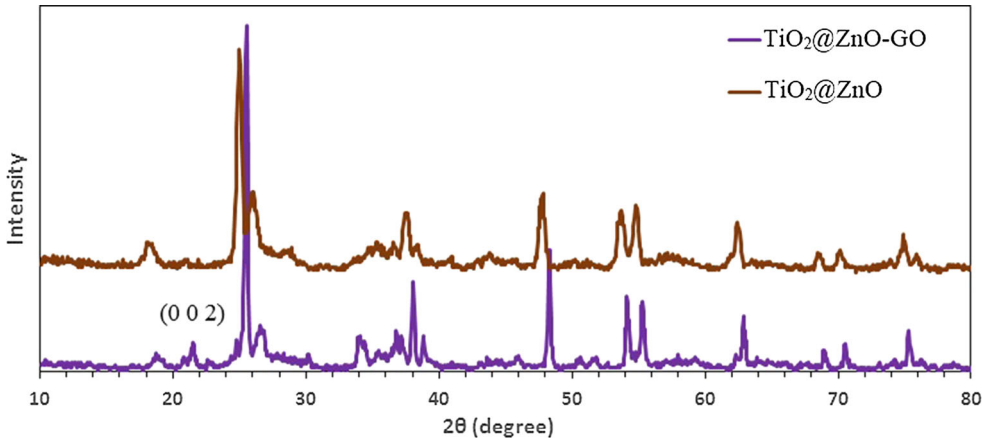

Figure 1 XRD pattern of nanocarriers.

(1 0 0), (0 0 2), (1 0 1), (1 0 2), (1 1 0), (1 0 3), and (1 1 2) planes, respectively. and the peaks of $2\theta = 25.6°$, 30.1°, 38.0°, 48.7°, and 54.1° can be indexed to the crystal faces of (1 0 1), (1 2 1), (0 0 4), (2 0 0), and (1 0 5) of TiO_2, respectively. Due to the low amount of graphene oxide in the composite, the (0 0 2) peak of the corresponding to an interlayer distance of GO nanosheets around 21° has slight intensity and shown in the inset Fig. 1 [41].

Particle morphology

Figure 2a, b shows the SEM image of TiO_2@ZnO–GO (a) and TiO_2@ZnO (b). TiO_2 nano particles are used as a template to produce fine ZnO powders. Last researches indicate that suitable amount of TiO_2 can effectively suppress grain growth and phase transformation of ZnO [42]. With this approach, we can produce uniform nanoparticles. It can be seen in Fig. 2a that the graphene nanosheets are fully exfoliated and almost decorated with nearly spherical TiO_2@ZnO nanoparticles. Figure 2b illustrates the SEM images of TiO_2@ZnO nanoparticles. It is evident from the Fig. 2b that the core–shell nanoparticles have a clear hexagonal phase with an average size of 190 nm. Figure 3 shows TEM images of TiO_2@ZnO core–shell nanoparticles, which show the agglomeration of particles with different shapes (both spherical and hexagonal shape can be observed). From TEM images, the average particle size was estimated to be around 190 nm for nanoparticles, which is consistent with the SEM results.

FT-IR analysis

FT-IR spectra of the NCs are shown in Fig. 4. Nevertheless, the significant bands that characterize the formation of TiO_2@ZnO are located at 470 and 657

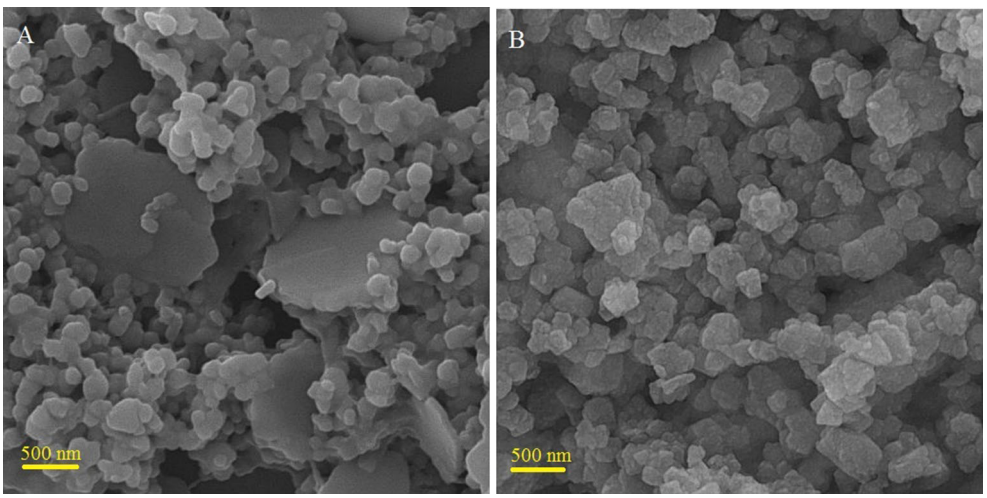

Figure 2 SEM images of TiO_2@ZnO–GO (A) and TiO_2@ZnO (B).

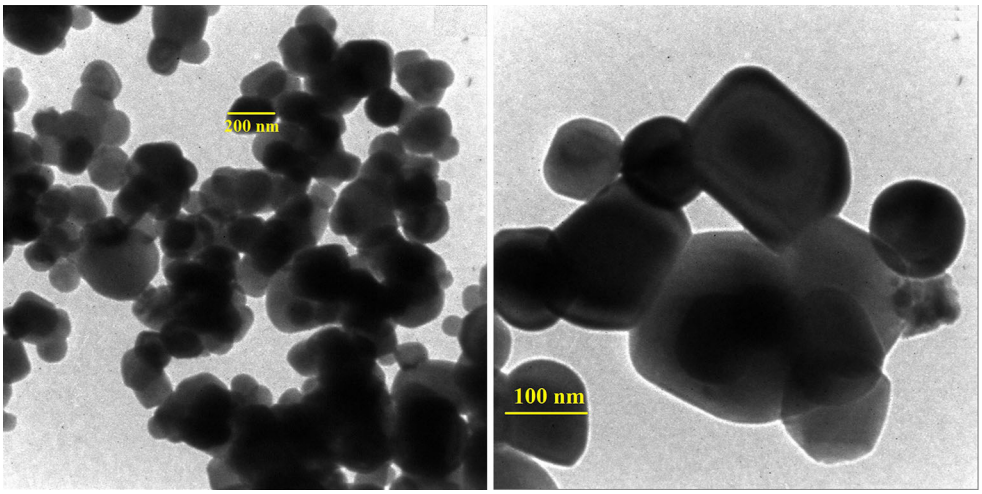

Figure 3 TEM images of TiO_2@ZnO.

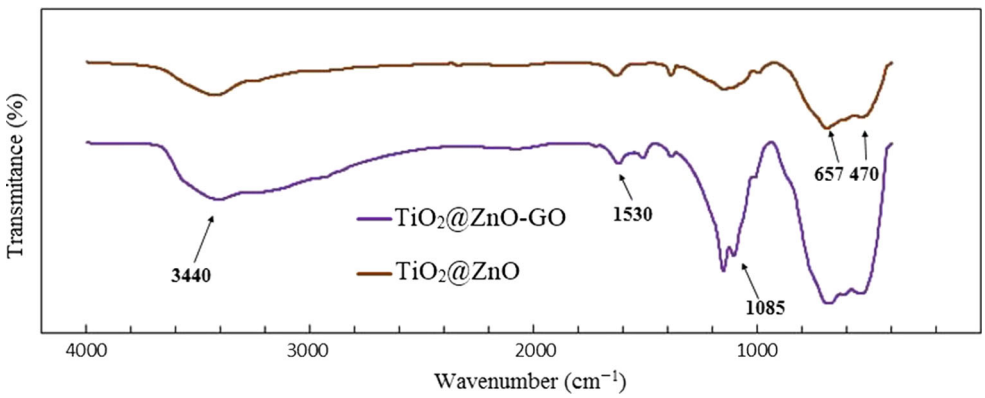

Figure 4 FT-IR curve of nanocarriers.

Wavenumber (cm^{-1}), which are associated with the vibrations of Zn–O and Ti–O bonds, respectively [43, 44]. The peaks at 1085, 1530 cm^{-1} were attributed to the stretching vibrations of C–O and C–H bonds, respectively [45]. In the case of the GO nanosheets, the absorption peak appeared at 3440 cm^{-1} in the IR spectra. This confirmed the presence of –OH groups in its nanostructure.

Surface charge of nanocarrier

The zeta potential of the aqueous suspension of NCs was also measured. Figure 5 shows zeta potential for TiO_2@ZnO–GO determined in the PBS buffer solution at pH 7.4 and 5.5, respectively. As shown in Fig. 5, zeta potential of CUR-loaded NCs at pH 7.4 and 5.5 was found to be about − 15.8 and − 0.31 mv. It is clear that at the pH 7.4 where our results showed a negative zeta potential due to carboxyl group of graphene oxide are ionized. At lower pH, the carboxyl group of graphene oxide are in deionized form which could form a proper condition for π–π stacking bond between drug and nanocarrier [46]. Surface charge is important in decisive whether the nanoparticles will cluster in blood flow or will stick to or interact with oppositely charged cell membrane. The plasma and blood cells constantly had a negative charge; nanoparticles with slight negative surface charge can minimize nonspecific contact with these components through electrostatic interactions [33, 47].

BET analysis

The nitrogen adsorption/desorption isotherms and pore size distribution profiles of TiO_2@ZnO are presented in Fig. 6. It can be seen, sample have microporous structure. The BET surface area and total pore volume of TiO_2@ZnO were calculated to be 31.59 m^2/g and 0.084 cm^3/g, respectively. As we

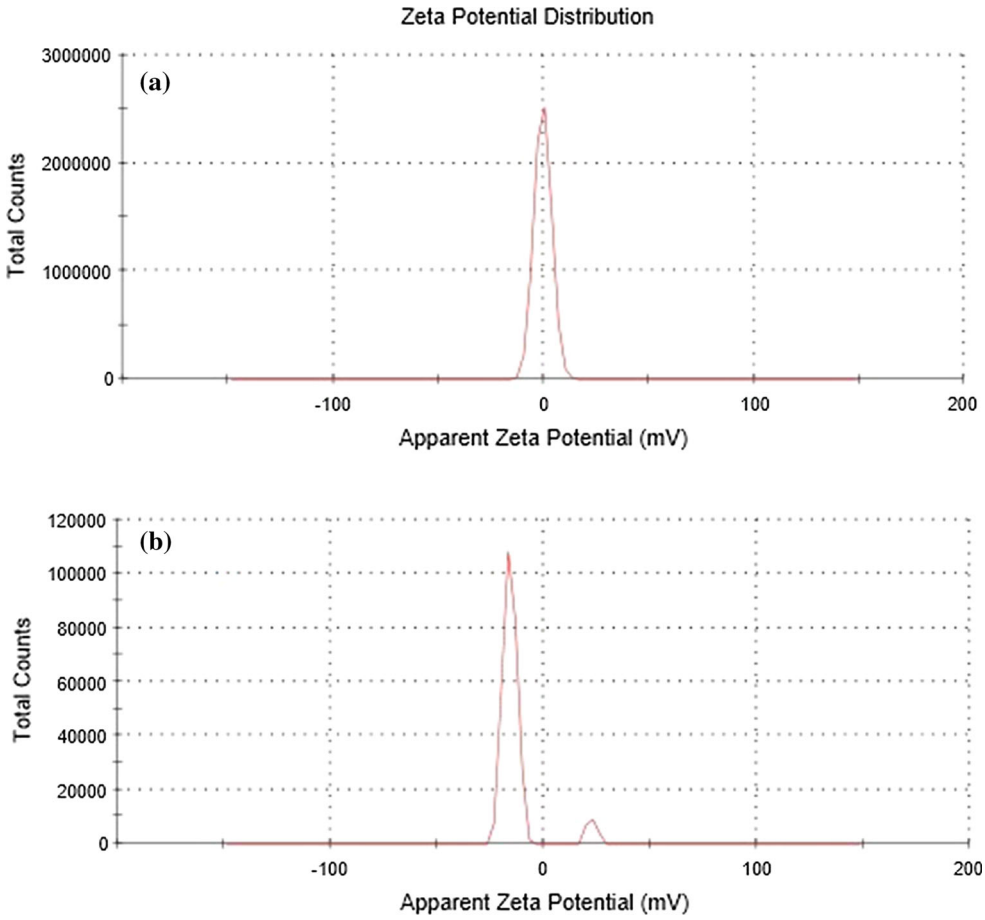

Figure 5 Zeta potential of TiO_2@ZnO–GO at PH 5.5 (**a**) and PH 7.4 (**b**).

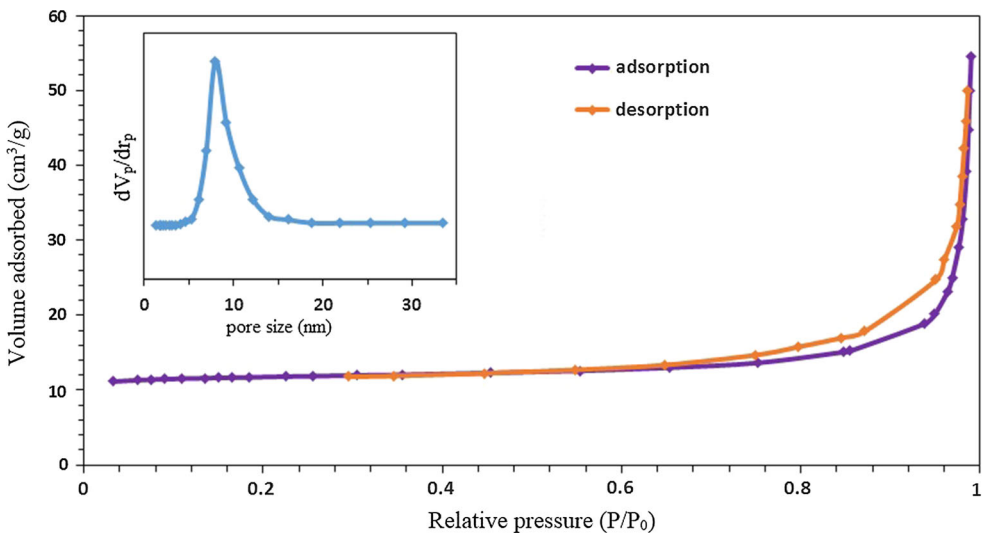

Figure 6 N_2 adsorption/desorption and pore size distribution of TiO_2@ZnO.

knew, the surface areas and pore volumes increased systematically with utilizing TiO_2. Similar trends were observed after loading or mixing TiO_2 with ZnO [48]. Researches showed that surface area of pure ZnO is about 11 m^2/g [49], so with this approach, surface area would be significantly higher than pure ZnO.

Drug loading and release study

The effect of TiO_2@ZnO and TiO_2@ZnO–GO on the loading and release of CUR were investigated in detail in this section. Figures 7 and 8 show a schematic diagram of CUR loading and release for NCs. The amounts of CUR incorporated as pure drug in these NCs are listed in Table 1. It is observed that the loading of CUR in the NCs increases when utilizing TiO_2@ZnO–GO instead of TiO_2@ZnO. This could be attributed to the strong π–π stacking interaction between GO and drugs, which allows the penetration of drug molecules into the NCs [46]. Figure 9 illustrates in vitro drug release profile of CUR-loaded in NCs at PH 5.5 and 7.4. The results revealed the bare curcumin release percents attainable after a period of 12 h in PBS pH 7.4 and 5.5 were 86 and 88%, respectively. As expected, percentage of CUR released from the NCs slightly increased as the pH value increased from 5.5 to 7.4. The drug release curve Fig. 9 clearly illustrates that at the 12-h, there is a 19 and 28% CUR release from TiO_2@ZnO to GO matrix which reached at 29s and 49% at pH 5.5 and 7.4, respectively, after six days. Sustained release of curcumin can be attributed to the entrapment of curcumin in mesoporous of NCs. The release is faster in neutral pH than acidic pH which can be attributed to deprotonation of residual carboxyl groups in GO of the TiO_2@ZnO–GO at higher pH, creating a repulsion force between the NC and the drug. Therefore, more amount of drug will be diffused out. In addition in neutral medium, the breaking of hydrogen bonding between the GO and CUR facilitated the release of the drug and thus increased the cumulative release. As expected, considerable initial

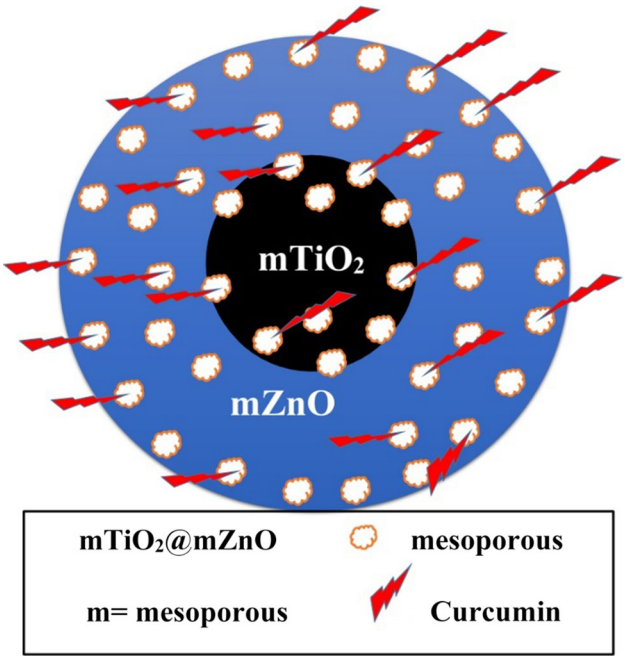

Figure 8 Schematic illustration of CUR in NCs.

Table 1 Drug loading of nanocarriers

Sample	Nanocarrier (μg)	Initial drug (μg)	DL%
TiO_2@ZnO	60000	15000	16.40
TiO_2@ZnO–GO	60000	15000	19.79

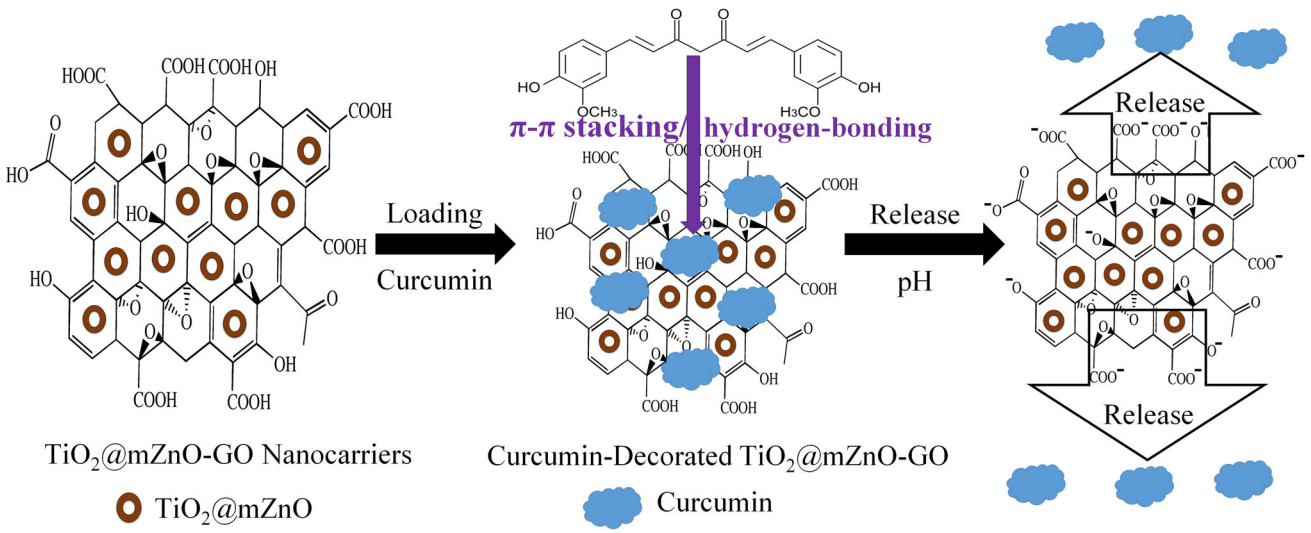

Figure 7 Schematic illustration of loading and release of CUR.

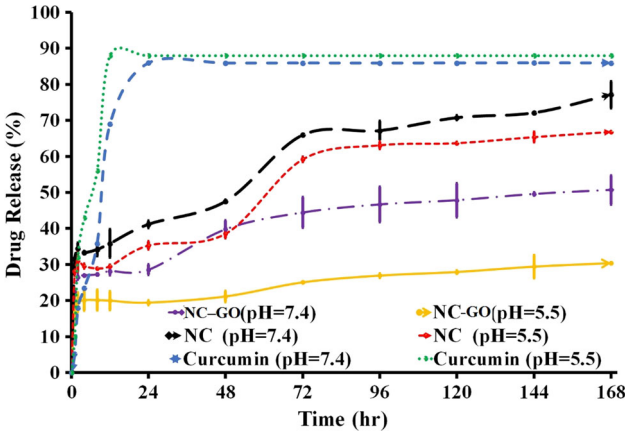

Figure 9 Release profiles at different pH values.

burst curcumin release was observed from the NCs due to desorbing curcumin from surface of NCs. This phenomenon could be useful for delivering drug to colon because after about 6 h the NCs reach to colon, therefore significant drug release should be happen during this period of time. In other hand, CUR released from NCs that could expose ZnO to cancer cells and bare ZnO makes this synergistic effect. These results reveal that TiO_2@ZnO–GO could be used as colon-specific drug delivery carriers that would show pH-dependent drug release behavior [50].

Study on cancerous cell's viability after CUR loaded TiO_2@ZnO and TiO_2@ZnO–GO NCs treatment

The in vitro anticancer effects of CUR-loaded NCs against human epithelial colorectal adenocarcinoma cells (Caco-2) (pH 6.2–6.9) estimated using a MTT assay (Fig. 10). MTT results illustrated that the Curcumin-loaded NCs showed significant toxicity due to which cell viability reduced to below 50% at 140 μg/mL concentration, thereby confirming its anticancer effect. The data exhibit that cell toxicity is directly proportionate to CUR-loaded NCs concentration. The concentration at which cell growth was inhibited by 50% (IC50) was specified by the standard curve method and is shown in Table 2. Higher toxicity of TiO_2@ZnO and TiO_2@ZnO–GO than CUR-loaded NCs can be imputed to the presence of ZnO nanoprecipitation on the cells. In particular, ZnO when reduced from bulk to nanoscale has been shown to exhibit inherent preferential cytotoxicity against cancer cells in vitro [51, 52]. Also, the cytotoxicity assay showed relatively higher toxicity of the TiO_2@ZnO than TiO_2@ZnO–GO against Caco-2 cancer cell lines. Therefore, GO reduced toxicity of ZnO nanoparticle. On other hand, curcumin-loaded NCs showed lower toxicity in the test revealed that adsorbed curcumin on surface of ZnO nanoparticles covered their surface and this method can reduce toxicity of ZnO nanoparticles. And due to lower

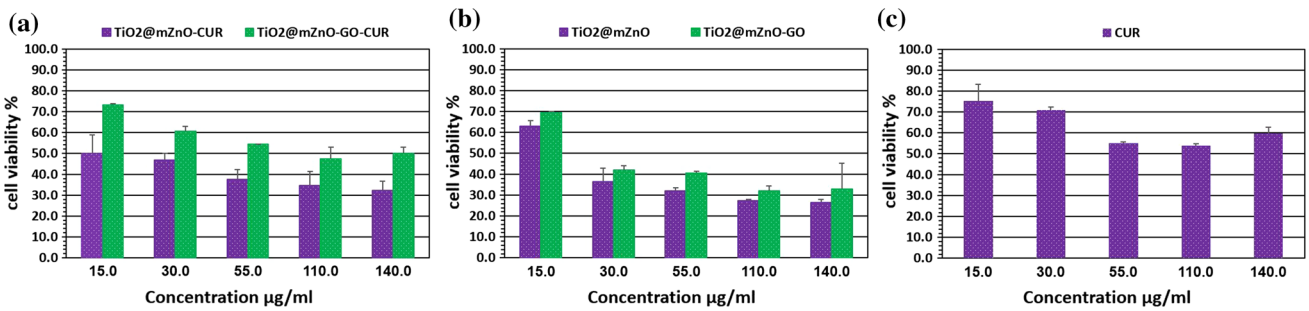

Figure 10 MTT assay for **a** CUR-loaded NCs, **b** bare NCs, and **c** void CUR on Caco-2 after incubation at 24 h. *X*-axes in figure are related to concentration of CUR and NCs, and *y*-axes show percentage of cell viability.

Table 2 Comparison of IC50 values for various concentration of void CUR and NCs at 24 h against Caco-2 cell line as determined by the MTT assay (the data unit is based on micromolar [μg/mL])

Type of treatment	TiO_2@ZnO–CUR	TiO_2@ZnO–GO–CUR	TiO_2@ZnO	TiO_2@ZnO–GO	CUR
IC 50	17.41	89.46	10.43	40.33	113.28

release of drugs in acidic environment like stomach, this method can protect normal cells of stomach against toxicity of ZnO. In other hand, when the physiological pH was increased (at colon), CUR released from NCs and bare ZnO makes this synergistic effect. Also, the comparable anticancer activity of NCs and curcumin revealed that curcumin retained its anticancer activity even after being loaded into NCs.

Conclusion

Novel TiO_2@ZnO–GO NC was synthesized as a pH-sensitive carrier for colon-targeted drug delivery. The SEM and TEM studies revealed that the prepared NCs had a diameter about 190 nm and hexagonal in shape. The TiO_2@ZnO–GO showed pH-dependent drug release behavior due to the presence of large amount of carboxylic acid group in the GO network. The release of CUR from the TiO_2@ZnO–GO was dependent on pH of the medium. It was found that the rate and amount of CUR released from the TiO_2@ZnO–GO are higher in pH 7.4. MTT results showed that the curcumin-loaded NCs showed significant toxicity due to which cell viability reduced to below 50% at 140 μg/mL concentration, thereby confirming its anticancer effects. These results demonstrate that TiO_2@ZnO–GO could be a drug delivery system to deliver the drug more specifically to the colon.

Compliance with ethical standards

Conflict of interest The authors declare that they have no conflict of interest.

References

[1] Yancik R, Ries LA (2000) Aging and cancer in America: demographic and epidemiologic perspectives. Hematol Oncol Clin North Am 14(1):17–23

[2] Schlüter K et al (2006) Organ-specific metastatic tumor cell adhesion and extravasation of colon carcinoma cells with different metastatic potential. Am J Pathol 169(3): 1064–1073

[3] Ko F-C et al (1999) Risk and patterns of brain metastases in colorectal cancer. Dis Colon Rectum 42(11):1467–1471

[4] Tournigand C et al (2012) Adjuvant therapy with fluorouracil and oxaliplatin in stage II and elderly patients (between ages 70 and 75 years) with colon cancer: subgroup analyses of the Multicenter International Study of Oxaliplatin, Fluorouracil, and Leucovorin in the Adjuvant Treatment of Colon Cancer trial. J Clin Oncol 30:3353–3360

[5] Danafar H et al (2017) Co-delivery of hydrophilic and hydrophobic drugs by micelles: a new approach using drug conjugated PEG–PCLNanoparticles. Drug Dev Ind Pharm 43(11):1908–1918

[6] Danafar H et al (2017) Investigation of drug delivery of rattle-structured gold nanorod-mesoporous silica nanoparticles core–shell as curcumin carrier and their effect on MCF7 and 4T1 cell lines. J Zanjan Univ Med Sci Health Serv 25(113):124–136

[7] Kheiri Manjili H et al (2017) Pharmacokinetics and in vivo delivery of curcumin by copolymeric mPEG-PCL micelles. Eur J Pharm Biopharm 116:17–30

[8] Danafar H (2017) Study of the composition of polycaprolactone/poly (ethylene glycol)/polycaprolactone copolymer and drug-to-polymer ratio on drug loading efficiency of curcumin to nanoparticles. Jundishapur J Nat Pharm Prod 12(1):e34179

[9] Sun Y-M et al (2002) Theoretical elucidation on the antioxidant mechanism of curcumin: a DFT study. Org Lett 4(17):2909–2911

[10] Panchatcharam M et al (2006) Curcumin improves wound healing by modulating collagen and decreasing reactive oxygen species. Mol Cell Biochem 290(1–2):87–96

[11] Sun A et al (2006) Synthesis of EF24-tripeptide chloromethyl ketone: a novel curcumin-related anticancer drug delivery system. J Med Chem 49(11):3153–3158

[12] Tønnesen HH, Karlsen J, van Henegouwen GB (1986) Studies on curcumin and curcuminoids VIII. Photochemical stability of curcumin. Z Lebensm Unters Forsch 183(2):116–122

[13] Tu H et al (2010) Study of the sigmoidal swelling kinetics of carboxymethylchitosan-g-poly (acrylic acid) hydrogels intended for colon-specific drug delivery. Carbohyd Polym 82(2):440–445

[14] Rao KM et al (2014) pH sensitive halloysite-sodium hyaluronate/poly (hydroxyethyl methacrylate) nanocomposites for colon cancer drug delivery. Appl Clay Sci 97:33–42

[15] Chuah LH et al (2014) Cellular uptake and anticancer effects of mucoadhesive curcumin-containing chitosan nanoparticles. Colloids Surf B 116:228–236

[16] Zhang L et al (2011) Eudragit® S100 coated calcium pectinate microspheres of curcumin for colon targeting. J Microencapsul 28(7):659–667

[17] Madan J et al (2014) Cyclodextrin complexes of reduced bromonoscapine in guar gum microspheres enhance colonic drug delivery. Mol Pharm 11(12):4339–4349

[18] Dutta RK, Sahu S (2012) Development of a novel probe sonication assisted enhanced loading of 5-FU in SPION encapsulated pectin nanocarriers for magnetic targeted drug delivery system. Eur J Pharm Biopharm 82(1):58–65

[19] Chen G-Y et al (2015) Graphene oxide as a chemosensitizer: diverted autophagic flux, enhanced nuclear import, elevated necrosis and improved antitumor effects. Biomaterials 40:12–22

[20] Novoselov K et al (2005) Two-dimensional atomic crystals. Proc Natl Acad Sci USA 102(30):10451–10453

[21] Calizo I et al (2007) Temperature dependence of the Raman spectra of graphene and graphene multilayers. Nano Lett 7(9):2645–2649

[22] Liu L et al (2008) Graphene oxidation: thickness-dependent etching and strong chemical doping. Nano Lett 8(7):1965–1970

[23] Huang JC (2002) Carbon black filled conducting polymers and polymer blends. Adv Polym Technol 21(4):299–313

[24] Ishigami M et al (2007) Atomic structure of graphene on SiO_2. Nano Lett 7(6):1643–1648

[25] Yan J et al (2007) Raman scattering and tunable electron–phonon coupling in single layer graphene. Solid State Commun 143(1):39–43

[26] Chen G-Y et al (2012) A graphene-based platform for induced pluripotent stem cells culture and differentiation. Biomaterials 33(2):418–427

[27] Zhang L et al (2010) Functional graphene oxide as a nanocarrier for controlled loading and targeted delivery of mixed anticancer drugs. Small 6(4):537–544

[28] Tao Y et al (2014) Immunostimulatory oligonucleotides-loaded cationic graphene oxide with photothermally enhanced immunogenicity for photothermal/immune cancer therapy. Biomaterials 35(37):9963–9971

[29] Chen GY et al (2014) Graphene oxide triggers toll-like receptors/autophagy responses in vitro and inhibits tumor growth in vivo. Adv Healthc Mater 3(9):1486–1495

[30] Danafar H et al (2017) Polylactide/poly(ethylene glycol)/polylactide triblock copolymer micelles as carrier for delivery of hydrophilic and hydrophobic drugs: a comparison study. J Pharm Investig. doi:10.1007/s40005-017-0334-8

[31] Nosrati H et al (2017) Green and one-pot surface coating of iron oxide magnetic nanoparticles (IONPs) with natural amino acids and its biocompatibility investigation. Appl Organomet Chem. doi:10.1002/aoc.4069

[32] Gharebaghi F et al (2017) Preparation of wormlike polymeric nanoparticles coated with silica for delivery of methotrexate and evaluation of anticancer activity against MCF7 cells. J Biomater Appl 31(9):1305–1316

[33] Nosrati H et al (2017) New advances strategies for surface functionalization of iron oxide magnetic nano particles (IONPs). Res Chem Intermed. doi:10.1007/s11164-017-3084-3

[34] Rasmussen JW et al (2010) Zinc oxide nanoparticles for selective destruction of tumor cells and potential for drug delivery applications. Expert Opin Drug Deliv 7(9):1063–1077

[35] Rahimi-Nasrabadi M et al (2016) Synthesis and characterization of $ZnFe_{2-x}Yb_xO_4$–graphene nanocomposites by sol–gel method. J Mater Sci Mater Electron 27(11):11940–11945

[36] Vallet-Regí M, Balas F, Arcos D (2007) Mesoporous materials for drug delivery. Angew Chem Int Ed 46(40):7548–7558

[37] Lopez T et al (2009) Kinetic study of controlled release of VPA and DPH antiepileptic drugs using biocompatible nanostructured sol–gel TiO_2. J Mater Sci 44(20):5459–5468. doi:10.1007/s10853-009-3745-8

[38] Hamadanian M, Rostami M, Jabbari V (2017) Graphene-supported C–N–S tridoped TiO_2 photo-catalyst with improved band gap and charge transfer properties. J Mater Sci Mater Electron 28(20):15637–15646

[39] Rostami M et al (2017) Facile synthesis and characterization of TiO_2–graphene–$ZnFe_{2-x}Tb_xO_4$ ternary nano-hybrids. J Mater Sci. doi:10.1007/s10853-017-0934-8

[40] Sun H et al (2014) A comparative study of reduced graphene oxide modified TiO_2, ZnO and Ta_2O_5 in visible light photocatalytic/photochemical oxidation of methylene blue. Appl Catal B 146:162–168

[41] Li M et al (2013) In situ synthesis and biocompatibility of nano hydroxyapatite on pristine and chitosan functionalized graphene oxide. J Mater Chem B 1(4):475–484

[42] Asl SK, Rad MK, Sadrnezhaad S (2011) Hydrothermal preparation of TiO_2–ZnO nano core-shell structure with quantum size effect. In: AIP conference proceedings, vol 1400. doi:10.1063/1.3663156

[43] Ganesh M et al (2012) Drug release evaluation of mesoporous TiO_2: a nano carrier for duloxetine. In: Computer applications for modeling, simulation, and automobile, vol 341. Springer, pp 237–243

[44] Anchieta CG et al (2014) Effects of solvent diols on the synthesis of $ZnFe_2O_4$ particles and their use as heterogeneous photo-Fenton catalysts. Materials 7(9):6281–6290

[45] Song M, Xu J (2013) Preparation of polyethylenimine-functionalized graphene oxide composite and its application in electrochemical ammonia sensors. Electroanalysis 25(2):523–530

[46] Upadhyaya L et al (2015) Efficient water soluble nanostructured ZnO grafted O-carboxymethyl chitosan/curcumin-nanocomposite for cancer therapy. Process Biochem 50(4):678–688

[47] Danafar H et al (2017) Drug-conjugated PLA–PEG–PLA copolymers: a novel approach for controlled delivery of hydrophilic drugs by micelle formation. Pharm Dev Technol 22(8):947–957

[48] Al-Johani MS, Al-Zaghayer Y, Al-Mayman SI (2015) TiO_2/ZnO photocatalytic activity for hydrogen production. Int Sci J Environ Sci 4:1–8

[49] Liang Y et al (2015) Preparation of porous 3D Ce-doped ZnO microflowers with enhanced photocatalytic performance. RSC Adv 5(74):59887–59894

[50] Seeli DS et al (2016) Guar gum succinate-sodium alginate beads as a pH-sensitive carrier for colon-specific drug delivery. Int J Biol Macromol 91:45–50

[51] Hanley C et al (2008) Preferential killing of cancer cells and activated human T cells using ZnO nanoparticles. Nanotechnology 19(29):295103

[52] Wang H et al (2009) Fluorescent dye encapsulated ZnO particles with cell-specific toxicity for potential use in biomedical applications. J Mater Sci Mater Med 20(1):11